Synthesis of Cold Antihydrogen in a Cusp Trap

Y. Enomoto,[1] N. Kuroda,[2] K. Michishio,[3] C. H. Kim,[2] H. Higaki,[4] Y. Nagata,[1] Y. Kanai,[1] H. A. Torii,[2] M. Corradini,[5] M. Leali,[5] E. Lodi-Rizzini,[5] V. Mascagna,[5] L. Venturelli,[5] N. Zurlo,[5] K. Fujii,[2] M. Ohtsuka,[2] K. Tanaka,[2] H. Imao,[6] Y. Nagashima,[3] Y. Matsuda,[2] B. Juhász,[7] A. Mohri,[1] and Y. Yamazaki[1,2]

[1]*RIKEN Advanced Science Institute, Hirosawa, Wako, Saitama 351-0198, Japan*
[2]*Graduate School of Arts and Sciences, University of Tokyo, Komaba, Meguro, Tokyo 153-8902, Japan*
[3]*Department of Physics, Tokyo University of Science, Kagurazaka, Shinjuku, Tokyo 162-8601, Japan*
[4]*Graduate School of Advanced Sciences of Matter, Hiroshima University, Kagamiyama, Higashi-Hiroshima, Hiroshima 739-8530, Japan*
[5]*Dipartimento di Chimica e Fisica per l'Ingegneria e per i Materiali, Università di Brescia & Istituto Nazionale di Fisica Nucleare, Gruppo Collegato di Brescia, 25133 Brescia, Italy*
[6]*RIKEN Nishina Center for Accelerator Based Science, Hirosawa, Wako, Saitama 351-0198, Japan*
[7]*Stefan Meyer Institute for Subatomic Physics, Austrian Academy of Sciences, 1090 Wien, Austria*

(Received 13 October 2010; published 7 December 2010)

We report here the first successful synthesis of cold antihydrogen atoms employing a cusp trap, which consists of a superconducting anti-Helmholtz coil and a stack of multiple ring electrodes. This success opens a new path to make a stringent test of the *CPT* symmetry via high precision microwave spectroscopy of ground-state hyperfine transitions of antihydrogen atoms.

DOI: 10.1103/PhysRevLett.105.243401 PACS numbers: 36.10.−k, 11.30.Er, 32.80.Ee, 52.27.Jt

Synthesis of antihydrogen ($\bar{H}$) atoms has been intensively studied in the last decades [1,2]. The primary physics goal is to make stringent tests of the *CPT* symmetry either via high precision laser spectroscopy of $1S$–$2S$ transition [3,4] or via high precision microwave spectroscopy of ground-state hyperfine transitions [5,6]. Recently, studies on the gravitational interaction of antimatter ($\bar{H}$) and matter (the Earth), the so-called weak-equivalence principle, are proposed [7] or under preparation [8]. The cold antimatter research celebrated an important milestone in 2002, when successful syntheses of cold $\bar{H}$ atoms in a uniform magnetic field were demonstrated by two research groups [9,10]. Both groups aim for $1S$–$2S$ high precision laser spectroscopy, and accordingly the next critical step is to prepare ultracold $\bar{H}$ atoms ($\lesssim 1$ K) in the low-field-seeking states and to trap them in the Ioffe-Pritchard trap or a variant of it having minimum B field configurations [11,12].

The present Letter reports successful synthesis of $\bar{H}$ atoms with a cusp trap scheme, which opens for the first time a path to realize high precision microwave spectroscopy of ground-state hyperfine transitions. In this case, the trapping of $\bar{H}$ atoms is not essential but an efficient extraction of a spin-polarized $\bar{H}$ beam is the key of the experiment [6]. Figure 1 is a conceptual drawing of an experimental setup for the microwave spectroscopy of $\bar{H}$ atoms, which consists of a cusp trap [the combination of a superconducting anti-Helmholtz coil and a stack of multiple ring electrodes (MRE)], a microwave cavity, a sextupole magnet, and a $\bar{H}$ detector. The cusp trap provides the minimum B field configuration still maintaining axially symmetric magnetic and electric fields. Because of this axial symmetry, the cusp trap realizes stable handlings of both antiprotons and positrons such as trapping, cooling, compression, and mixing [13,14]. It is expected that $\bar{H}$ atoms in the low-field-seeking (LFS) states are preferentially focused along the cusp trap axis whereas those in the high-field-seeking (HFS) states are strongly defocused, resulting in the formation of an intensity enhanced highly spin-polarized $\bar{H}$ beam [6]. Our preliminary simulation revealed that the polarization of 50 K $\bar{H}$ beam amounts to about 30% when they are synthesized near the maximum magnetic field in the cusp trap [15]. The microwave cavity induces hyperfine transitions from LFS to HFS states when the microwave frequency is in resonance. The sextupole magnet sorts out $\bar{H}$ atoms in HFS states from those in LFS states. Another advantage of the cusp trap scheme is the fact that the microwave cavity can be installed in a weak uniform magnetic field away from the $\bar{H}$ formation trap, which enables high precision spectroscopy of $\bar{H}$ atoms.

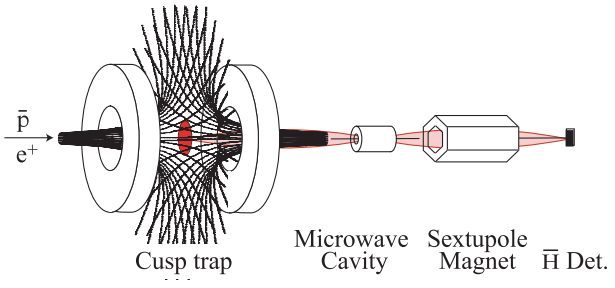

FIG. 1 (color online). A conceptual experimental setup for the ground-state hyperfine transition measurements of $\bar{H}$ atoms with the cusp trap (see the text for more details).

This is not necessarily the case for trapped $\bar{H}$ atoms in a strong nonuniform magnetic field [16].

Figure 2 schematically shows the present experimental setup used for the $\bar{H}$ synthesis, which consists of the antiproton ($\bar{p}$) catching trap [17], the compact positron (e^+) accumulator [18], the cusp trap, the 3D track detector [19], and the $\bar{H}$ detector. Antiprotons of 5.3 MeV from the antiproton decelerator (AD) at CERN were extracted into the ASACUSA area, slowed down to 120 keV by a radio frequency quadrupole decelerator (RFQD), and then were injected into the $\bar{p}$ catching trap through a double thin degrader foil of 180 μg/cm^2 thickness. About 10^6 antiprotons were accumulated and electron-cooled per one AD shot in the $\bar{p}$ catching trap. The antiproton cloud was radially compressed [20] for efficient transportation into the cusp trap. The compact e^+ accumulator was designed and developed for this research [18]. A 27 mCi ^{22}Na positron source and an MRE for positrons were installed in a cryogenic bore tube of a superconducting solenoid operated at 2.5 T (total length of 2 m). The 3D track detector consisted of two pairs of two modules each having 64 horizontal and 64 vertical scintillator bars of 1.5 cm width. It was used to determine the annihilation position of antiprotons by monitoring charged pion trajectories.

Figure 3(a) is a drawing of an MRE in the cusp trap for $\bar{H}$ synthesis (MRE$_{\bar{H}}$), which consists of 17 ring electrodes including two four-segmented electrodes ($U4$ and $D4$) for the radial compression of a positron plasma. The ring electrodes have a relatively large inner diameter (80 mm) for efficient extraction of $\bar{H}$ atoms. The MRE$_{\bar{H}}$ was installed in a cryogenic bore tube (6 K) [21] of the superconducting anti-Helmholtz coil (the maximum magnetic field along the axis was 2.7 T), and was cooled via heat conduction down to about 15 K. The MRE$_{\bar{H}}$ and the anti-Helmholtz coil were aligned to the beam axis (z axis) with its central electrode [CE in Fig. 3(a)] at the symmetry point of the cusp magnetic field ($B = 0$). Figure 3(b) draws the magnetic field along the beam axis.

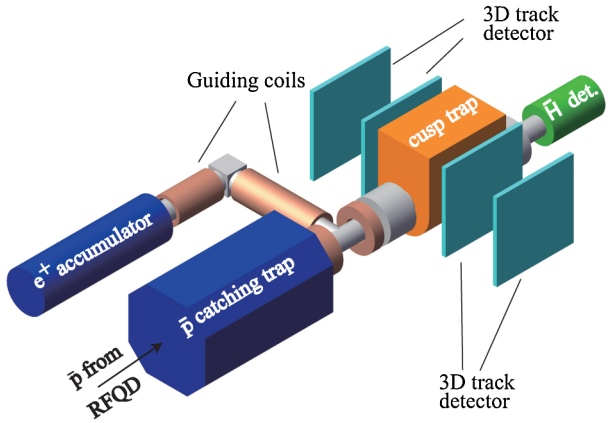

FIG. 2 (color online). A schematic drawing of the present experimental setup, which consists of the antiproton ($\bar{p}$) catching trap, the compact positron (e^+) accumulator, the cusp trap for antihydrogen ($\bar{H}$) synthesis, the 3D track detector, and the $\bar{H}$ detector downstream of the cusp trap.

The procedure to synthesize and detect $\bar{H}$ atoms consisted of the following six steps: (i) Positrons of about 100 eV with a pulse width of about 30 ns were extracted from the e^+ accumulator, transported with the guiding coils (see Fig. 2), and injected into the upstream part of the MRE$_{\bar{H}}$ with a potential configuration ϕ_1 in Fig. 3(c). Immediately after the injection, the potential was switched to ϕ_2. Positrons were spontaneously cooled via synchrotron radiation to an environmental temperature within a few seconds and formed a non-neutral plasma. When necessary, these trapping and cooling procedures were repeated to accumulate more positrons. (ii) The positron plasma was compressed to less than 3 mm in diameter (the density $\rho_{e^+} \sim 10^7/\text{cm}^3$ [22]) by a rotating electric field applied via $U4$ [13]. (iii) The potential was smoothly varied from ϕ_2 to ϕ_3 [see Fig. 3(c)] with the positron plasma kept compressed at the center of the nested potential. The potential at the center of the nested trap was tuned to be -147 V. (iv) Antiprotons of about 150 eV with a pulse width of about 2 μs were injected from the $\bar{p}$ catching trap into the MRE$_{\bar{H}}$ with the potential ϕ_4. Immediately after the injection, the potential was switched back to ϕ_3 so that the antiprotons were confined in the nested trap and mixed with the preloaded positrons. Positrons were heated by injected antiprotons, then cooled via synchrotron radiation, and eventually captured by antiprotons to form $\bar{H}$ atoms. Although antiprotons in the nested trap had no chance to move beyond the nested potential, $\bar{H}$ atoms

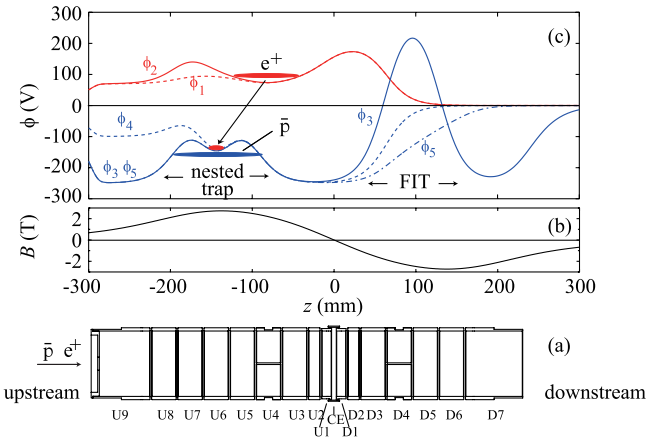

FIG. 3 (color online). (a) A drawing of the stack of multiple ring electrodes of the cusp trap (MRE$_{\bar{H}}$). (b) The magnetic field $B(T)$ along the beam axis. (c) The electric potential $\phi(z)$ along the beam axis. The potential ϕ_1 for injection of positrons. ϕ_2 for accumulation and compression of positrons. ϕ_3 for mixing of antiprotons and positrons. [The mixing region in the upstream part is called the nested trap, and the harmonic part in the downstream is called the field-ionization trap (FIT).] ϕ_4 for antiproton injection from the upstream side. ϕ_5 for extraction of antiprotons accumulated in the FIT originating from the field-ionized $\bar{H}$ atoms.

moved freely because they are neutral, and a part of them reached the field-ionization trap (FIT). If $\bar{H}$ atoms were formed via three-body-recombination process in high Rydberg states, they were field ionized and their antiprotons were accumulated in the FIT [10]. (v) The FIT was repeatedly opened like ϕ_5 for 100 ms every 5 s for 20 times. Antiprotons accumulated in the FIT over the 5 s period were released and annihilated each time the FIT was opened. The 3D track detector was used to monitor the antiproton annihilation with the detection efficiency of almost 100%. (vi) The potential was switched to ϕ_2.

Figure 4 shows the counts from the 3D track detector during mixture of antiprotons (a) with and (b) without positrons at the step (v). It is seen that a sharp peak of a fraction of ms width appeared at $t_{\mathrm{FIT}} = 0$ only if positrons were in the nested trap. The weak background was primarily due to the annihilation of trapped antiprotons with the residual gas. It is also noted that the peak height was considerably reduced when the positrons in the nested trap were heated by a weak RF field [9] applied via the electrode $U4$. These findings confirm the synthesis of $\bar{H}$ atoms.

Figure 5(a) shows the number of antiprotons accumulated in the FIT every 5 s as a function of time since the start of the mixture of 3×10^5 antiprotons in 3×10^6 positrons. The number increased in the first 30 s and then slowly decreased in the next 80 s yielding totally 70 antiprotons per mixture. Assuming an isotropic angular distribution of $\bar{H}$ atoms and taking into account the solid angle covered by the FIT, the total number of $\bar{H}$ atoms in high Rydberg states was estimated to be about 7×10^3 per mixture. In other words, the $\bar{H}$ formation efficiency was about 2%.

We changed the number of antiprotons for the same number of positrons to see how it makes a difference to the time dependence of the number of field-ionized $\bar{H}$ atoms. As the number of antiproton was decreased (increased), the synthesis rate peaked earlier (later) and the synthesis period became shorter (longer). This observation is consistent with an expectation that the cooling of heated positrons proceeds faster for smaller number of antiprotons. We also noticed that the probability of the $\bar{H}$ synthesis was higher for smaller number of incident antiprotons. For example, the $\bar{H}$ formation efficiency was about 7% for 4×10^4 antiprotons. Figures 5(b) and 5(c) show the annihilation position distribution of antiprotons along the beam axis measured with the 3D track detector for $0\ \mathrm{s} < t < 60\ \mathrm{s}$ and $60\ \mathrm{s} < t < 120\ \mathrm{s}$, respectively. A sharp single peak is seen in Fig. 5(b) near the positron trapping position ($z = -144$ mm). The peak gets broader for Fig. 5(c) with an indication of two bumps near the potential maxima of the nested trap ($z = -175$ mm and $z = -113$ mm). The latter observation showed that antiprotons were axially separated from the e^+ plasma after several tens of seconds. This axial separation can explain why the $\bar{H}$ synthesis rate decreased and almost disappeared after 100 s although a large number of antiprotons and positrons were still left in the nested trap.

In order to estimate the principal quantum number n of the synthesized $\bar{H}$ atoms, the field strength of the FIT was tuned by varying the voltage on the electrodes $D4$ and $D5$. The solid circles in Fig. 6 show the number of field-ionized $\bar{H}$ atoms as a function of the voltage applied to $D4$ and $D5$ (The potential ϕ_3 in Fig. 3(c) corresponds to $V_{D4,5} = 350$ V). It is seen that the number of field-ionized $\bar{H}$ atoms increased as $V_{D4,5}$ increased, and then saturated. We calculated the probability for $\bar{H}$ atoms to be field ionized and accumulated in the FIT, assuming they were in a specific n state and drifting out isotropically from the center of the nested trap. We adopted a semiquantitative formula for the field ionization neglecting influences of the magnetic field

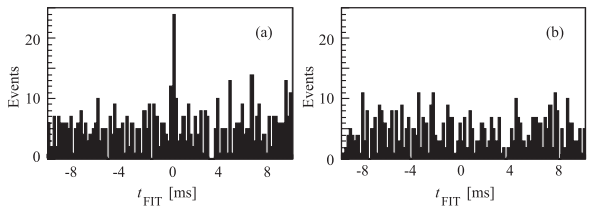

FIG. 4. The time spectra obtained by summing the spectra around the timing of the first ten FIT openings ($-10\ \mathrm{ms} < t_{\mathrm{FIT}} < 10\ \mathrm{ms}$) (a) with and (b) without positrons. A sharp peak is seen at $t_{\mathrm{FIT}} = 0$ only when positrons were in the nested trap.

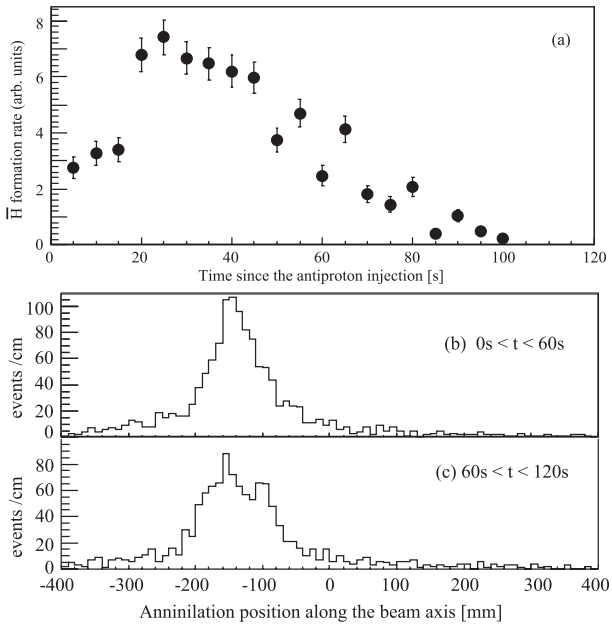

FIG. 5. (a) The number of field-ionized antihydrogen atoms accumulated in the FIT monitored by opening the FIT every 5 s. Each data point was obtained repeating the steps from (ii) to (iv) for 19 times. (b),(c) The annihilation position distributions observed by the 3D track detector for $0\ \mathrm{s} < t < 60\ \mathrm{s}$ and $60\ \mathrm{s} < t < 120\ \mathrm{s}$, respectively.

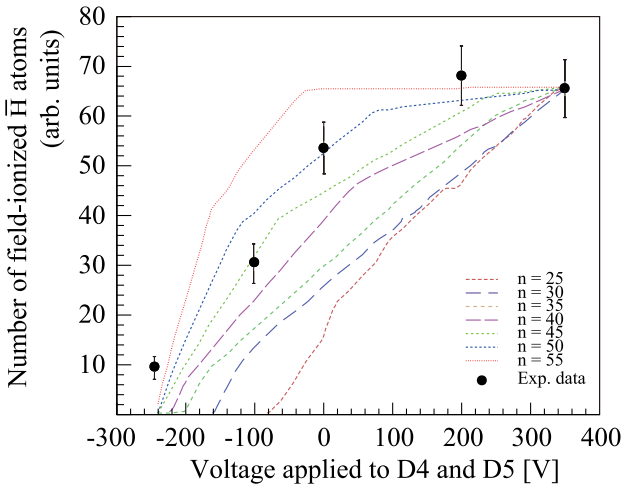

FIG. 6 (color online). The number of field-ionized $\bar{H}$ atoms as a function of the voltage applied on the electrodes $D4$ and $D5$ ($V_{D4,5}$). The solid circles show the experimental results. Seven curves correspond to field-ionization probabilities of $\bar{H}$ atoms calculated for $25 \leq n \leq 55$. The probabilities are scaled to the experimental value at 350 V.

for the sake of simplicity, $F \sim 3.2 \times 10^8 n^{-4}(\mathrm{V/cm})$ [23], where F is the minimum field strength at which the atom in the n state is field ionized. Seven curves in Fig. 6 show such probabilities for $25 \leq n \leq 55$ taking into account the electric field strength experienced by $\bar{H}$ atoms along their trajectories in the $\mathrm{MRE}_{\bar{H}}$. The present observation is consistent with the curve for $n \sim 45$ and/or 50. It is noted that $\bar{H}$ atoms with $n \gtrsim 55$ are field ionized by the electric field of the nested trap before they reach the FIT. In the case of three body recombination processes, a typical n can be crudely estimated as $n \sim 400/\sqrt{T(K)}$ by equating the binding energy and the positron temperature. The temperature of the positron plasma during the experiments was then estimated to be several tens of kelvins, which was consistent with a leak mode temperature measurement developed in Ref. [24].

Summarizing, we demonstrated the successful synthesis of cold antihydrogen atoms employing a cusp trap. This success opens for the first time a realistic path to make a stringent test of the *CPT* symmetry with an extracted $\bar{H}$ beam. In the present configuration, the formation efficiency from antiprotons to $\bar{H}$ atoms in high Rydberg states was typically 2% (maximum 7%) of the injected antiprotons. We are in a process of optimizing the extraction parameters for a spin-polarized cold $\bar{H}$ beam along the cusp trap axis and of making the microwave spectroscopy. It is also noted that the self-cooling and ground-state antihydrogen atom formation predicted in [15] would play an important role when the nested trap is prepared near the center of the $\mathrm{MRE}_{\bar{H}}$.

We would like to thank CERN, the AD team, and the RF team for their great efforts and support. This work was supported by the Grant-in-Aid for Specially Promoted Research (19002004) of the Japanese Ministry of Education, Culture, Sports, Science and Technology (MonbuKagaku-shō), Special Research Projects for Basic Science of RIKEN, Università di Brescia (Italy), and Istituto Nazionale di Fisica Nucleare (Italy).

[1] G. Gabrielse, Adv. At. Mol. Opt. Phys. **50**, 155 (2005).
[2] M. Charlton *et al.*, Phys. Rep. **241**, 65 (1994).
[3] ATRAP Collaboration, Tech. Rep. SPSC-P-306, CERN CERN-SPSC 97-8, Geneva, 1997.
[4] ALPHA Collaboration, Tech. Rep. SPSC-P-325, CERN CERN-SPSC 2005-006, Geneva, 2005
[5] ASACUSA Collaboration, Tech. Rep. SPSC-P-307 Add. 1, CERN-SPSC 2005-002, Geneva, 2005; B. Juhász and E. Widmann, Hyperfine Interact. **193**, 305 (2009).
[6] A. Mohri and Y. Yamazaki, Europhys. Lett. **63**, 207 (2003).
[7] AEGIS Collaboration, Tech. Rep. SPSC-P-334, CERN CERN-SPSC 2007-017, Geneva, 2007.
[8] P. Perez *et al.*, AIP Conf. Proc. **1037**, 35 (2008).
[9] M. Amoretti *et al.*, Nature (London) **419**, 456 (2002).
[10] G. Gabrielse *et al.*, Phys. Rev. Lett. **89**, 213401 (2002).
[11] G. Gabrielse *et al.*, Phys. Rev. Lett. **100**, 113001 (2008).
[12] G. B. Andresen *et al.*, Phys. Lett. B **685**, 141 (2010).
[13] H. Saitoh, A. Mohri, Y. Enomoto, Y. Kanai, and Y. Yamazaki, Phys. Rev. A **77**, 051403(R) (2008).
[14] A. Mohri, H. Saitoh, Y. Kanai, and Y. Yamazaki, in *Proceedings of the 33rd EPS Conference on Plasma Physics* (EPS, London, 2006), p. 4.067.
[15] The cusp trap can also confine cold $\bar{H}$ atoms in the LFS states with an efficient cooling mechanism. See, e.g., T. Pohl, H. R. Sadeghpour, Y. Nagata, and Y. Yamazaki, Phys. Rev. Lett. **97**, 213001 (2006).
[16] T. W. Hänsch and C. Zimmermann, Hyperfine Interact. **76**, 47 (1993).
[17] N. Kuroda *et al.*, Phys. Rev. Lett. **94**, 023401 (2005).
[18] H. Imao *et al.*, Hyperfine Interact. **194**, 71 (2009).
[19] M. Corradini *et al.* (to be published).
[20] N. Kuroda *et al.*, Phys. Rev. Lett. **100**, 203402 (2008).
[21] M. Shibata, A. Mohri, Y. Kanai, Y. Enomoto, and Y. Yamazaki, Rev. Sci. Instrum. **79**, 015112 (2008).
[22] This positron density was before the antiproton injection. An abrupt radial expansion was seen after the injection.
[23] T. F. Gallagher, *Rydberg Atoms* (Cambridge University Press, New York, 1994).
[24] B. R. Beck, J. Fajans, and J. Malmberg, Phys. Rev. Lett. **68**, 317 (1992).